Multiple-spin coherence transfer in linear Ising spin chains and beyond: Numerically optimized pulses and experiments

Manoj Nimbalkar,[1,*] Robert Zeier,[1,†] Jorge L. Neves,[1,2] S. Begam Elavarasi,[1,3] Haidong Yuan,[4,5] Navin Khaneja,[5] Kavita Dorai,[6] and Steffen J. Glaser[1,‡]

[1]*Department Chemie, Technische Universität München, Lichtenbergstrasse 4, 85747 Garching, Germany*
[2]*Laboratorio de Genomica Estrutural, Instituto de Biofísica Carlos Chagas Filho, Universidade Federal do Rio de Janeiro, Rio de Janeiro, Rio de Janeiro 21941-590, Brazil*
[3]*B. S. Abdur Rahman University, Seethakathi Estate, Vandalur, Chennai 600048, India*
[4]*Department of Mechanical Engineering, Massachusetts Institute of Technology, 77 Massachusetts Avenue, Cambridge, Massachusetts 02139, USA*
[5]*School of Engineering and Applied Sciences, Harvard University, 33 Oxford Street, Cambridge, Massachusetts 02138, USA*
[6]*IISER Mohali, MGSIPAP Complex, Sector 26, Chandigarh 160019, India*

We study multiple-spin coherence transfers in linear Ising spin chains with nearest-neighbor couplings. These constitute a model for efficient information transfers in future quantum computing devices and for many multidimensional experiments for the assignment of complex spectra in nuclear magnetic resonance spectroscopy. We complement prior analytic techniques for multiple-spin coherence transfers with a systematic numerical study where we obtain strong evidence that a certain analytically motivated family of restricted controls is sufficient for time optimality. In the case of a linear three-spin system, additional evidence suggests that prior analytic pulse sequences using this family of restricted controls are time optimal even for arbitrary local controls. In addition, we compare the pulse sequences for linear Ising spin chains to pulse sequences for more realistic spin systems with additional long-range couplings between nonadjacent spins. We experimentally implement the derived pulse sequences in three- and four-spin systems and demonstrate that they are applicable in realistic settings under relaxation and experimental imperfections—in particular—by deriving broadband pulse sequences which are robust with respect to frequency offsets.

I. INTRODUCTION

The control of spin dynamics in chains of coupled spins $1/2$ is a topic of both theoretical and practical interest [1–12]. On the one hand, the use of spin chains is considered for the efficient transfer of information in future quantum computing devices [13–19]. On the other hand, coherence transfer between remote spins is the basis of many multidimensional experiments for the assignment of complex spectra [20–22] in nuclear magnetic resonance (NMR) spectroscopy. In addition to linear spin chains with only nearest-neighbor couplings, in realistic settings long-range couplings between nonadjacent spins must also be considered. For example, in ^{13}C- and ^{15}N-labeled proteins, the nuclei in the protein backbone form a chain of coupled spins $1/2$ with dominant next-neighbor ^1J (single-bond) couplings and smaller ^2J and ^3J couplings (via two or three chemical bonds) between nonadjacent spins in the chain [22].

Here we focus on the efficient creation of multispin operators from a single-spin operator in a spin chain, such as the creation of multiple-spin order from polarization of the first spin,

$$I_{1z} \rightarrow 2^{n-1} I_{1z} I_{2z} \cdots I_{(n-1)z} I_{nz}. \tag{1}$$

The transfer shown in Eq. (1) is just a prototype example of a general transfer of the form

$$I_{1\delta} \rightarrow 2^{n-1} I_{1\epsilon_1} \cdots I_{n\epsilon_n}, \tag{2}$$

where $\delta, \epsilon_k \in \{x, y, z\}$ for $k = 1, \ldots, n$. Note that the transformations in Eqs. (1) and (2) are identical up to local spin rotations. Hence, in the limit where the time for selective rotations of individual spins is negligible [compared to $1/(2J_{\max})$, where $J_{\max}$ is the largest spin-spin coupling constant in the chain], the transformations in Eqs. (1) and (2) can be achieved in the same amount of time. (This situation is typical for heteronuclear NMR experiments in the liquid state, where the control amplitudes for single-spin operators are orders of magnitude larger than the largest coupling constants.) In Eq. (2), the initial single-spin state is not limited to longitudinal magnetization (polarization I_{1z}) but may also be transverse magnetization (in-phase coherence I_{1x} or I_{1y}) [22,23]. Examples of multispin target operators in Eq. (2) containing one or several transverse operators include states of the form $2^{n-1} I_{1z} I_{2z} \cdots I_{(n-1)z} I_{nx}$ (corresponding to antiphase coherence of spin n with respect to spins 1 to $n - 1$), and $2^{n-1} I_{1x} I_{2x} \cdots I_{(n-1)x} I_{nx}$ (corresponding to multiquantum coherence), which are relevant in so-called "out and back" transfer schemes [22,24,25] and in the creation of multiple-quantum coherence [23,26], respectively.

We consider in this work only the case of Ising-type spin chains [27,28]. In NMR, an Ising-type coupling is also known as *weak coupling*, as only Ising-type couplings need to be

---

*manoj.nimbalkar@tum.de
†robert.zeier@ch.tum.de
‡steffen.glaser@tum.de

considered if the coupling constant $J_{k\ell}$ between two spins k and ℓ is much smaller than the difference between the resonance frequencies ν_k and ν_ℓ of these two spins, i.e., if $|J_{k\ell}| \ll |\nu_k - \nu_\ell|$ [23]. This is an excellent approximation in virtually all high-resolution heteronuclear NMR experiments (where the gyromagnetic ratios of the spins are different) as $|J_{k\ell}|/|\nu_k - \nu_\ell| \leqslant 10^{-6}$ holds in modern high-field NMR spectrometers. We obtain that the coupling Hamiltonian for a pair of spins k and ℓ has the form

$$H_{k\ell}^{\text{weak}} = 2\pi J_{k\ell} I_{kz} I_{\ell z},$$

where $J_{k\ell}$ is the coupling constant in units of hertz. In conventional experiments, the standard methods to achieve transfer in Eq. (2) are based on COSY- or RELAY-type transfer steps [22,23], which are realized in heteronuclear experiments by a series of INEPT building blocks [29] (see Sec. II). The transfer time is determined by the size of the coupling constants $J_{k\ell}$ in a given spin system. For example, in a linear spin chain with only next-neighbor couplings, the total duration is given by

$$T_{\text{conv}} = \left(J_{12}^{-1} + J_{23}^{-1} + \cdots + J_{(n-1)n}^{-1} \right)/2.$$

We are interested in finding the shortest possible time to achieve the transfer in Eq. (2) or, conversely, the maximum transfer amplitude for any given time, which remains an open question up to now.

For relatively simple spin systems, consisting of up to three spins, time-optimal [30–36] and relaxation-optimized [37–42] pulse sequences have been recently found analytically, based on methods of optimal control theory [43–47], establishing rigorous physical limits for minimum transfer times or minimum relaxation losses, respectively. In addition to powerful analytical tools, optimal control theory also provides efficient numerical algorithms for the optimization of pulse sequences, such as the gradient ascent pulse engineering (GRAPE) algorithm, exploiting the known equation of motion for the spin system [48–51]. With this algorithm it is possible to optimize tens of thousands of pulse sequence parameters, and the resulting pulse sequences are not limited to previously known transfer schemes. However, in contrast to analytical methods proving global optimality of a given pulse sequence, there is no guarantee that numerical optimal control algorithms like GRAPE will converge to the global optimum [52]. Nevertheless, in cases where the theoretical limits are known, the GRAPE algorithm closely approached these limits [48,53]. This motivated its use also in cases for which analytical results on the global optimum are presently unknown in order to explore the physical limits of the maximum possible transfer efficiency as a function of transfer time, resulting in so-called time-optimal pulse (TOP) curves [46,54–58]. Furthermore, additional effects such as relaxation [59,60], radiation damping [61], and experimental constraints and imperfections—like limited control amplitudes and control field inhomogeneities [62–64]—can be taken into account to find highly robust pulses suitable for practical applications under realistic conditions.

Assuming a restricted pulse structure (see Secs. III A and IV A), analytical pulses were derived in Refs. [11,12], respectively, for the cases of equal and unequal couplings. This results in significantly shorter transfer times compared to

conventional approaches; however, it was not clear how closely the performance of the derived pulse sequences converges to the time-optimal performance.

In this work, we summarize the analytic approach of Refs. [11,12] (see Secs. III A and IV A) and explore its time optimality by conducting a systematic numerical study of the considered coherence transfer (see Secs. III B and IV B). Focusing on the case of linear Ising spin chains with three and four qubits, we compare the duration of pulse sequences for arbitrary pulse structures with the restricted pulse structure motivated by the analytical pulses. We also discuss qualitatively in Sec. IV B the results of our numerical optimizations. In addition, we numerically analyze linear Ising spin chains for up to six spins (see Sec. VII). Our numerical approach makes it also possible to investigate more realistic spin systems with more general coupling topologies (see Sec. V).

We show in Sec. VI how to make the pulse sequences robust with respect to off-resonance effects using the delays alternating with nutations for tailored excitation (DANTE) approach [34,65,66]. Finally, we present experimental results for model spin chains consisting of three and four heteronuclear spins 1/2, demonstrating good performance of these sequences under experimental conditions and comparing the results to those for conventional pulse sequences.

II. COHERENCE TRANSFER IN LINEAR ISING SPIN CHAINS

Throughout this work we mostly consider linear Ising spin chains which have only direct couplings between neighboring spins [27,28]. (Later we will also allow additional couplings between non-neighboring spins.) Assume that a chain of n spins is placed in a static external magnetic field along the z direction and that neighboring spins are coupled by an Ising interaction where the coupling strengths $J_{\ell,\ell+1}$ are fixed but may depend on the position $1 \leqslant \ell \leqslant n-1$ in the chain. Without any control, the system evolves freely under its drift Hamiltonian

$$H_d = 2\pi \sum_{\ell=1}^{n-1} J_{\ell,\ell+1} I_{\ell z} I_{(\ell+1)z}.$$

The drift Hamiltonian is given in a suitably chosen multiple rotating frame, which rotates simultaneously at the resonance frequency of each spin. We use the product-operator basis $I_{\ell \nu} = \otimes_j I_{a_j}$ where $a_j = \nu$ for $j = \ell$ and $a_j = 0$ otherwise (see Ref. [23]). The matrices $I_x := \left(\begin{smallmatrix} 0 & 1 \\ 1 & 0 \end{smallmatrix} \right)/2$, $I_y := \left(\begin{smallmatrix} 0 & -i \\ i & 0 \end{smallmatrix} \right)/2$, and $I_z := \left(\begin{smallmatrix} 1 & 0 \\ 0 & -1 \end{smallmatrix} \right)/2$ are the Pauli spin matrices and $I_0 := \left(\begin{smallmatrix} 1 & 0 \\ 0 & 1 \end{smallmatrix} \right)$ is the (2×2)-dimensional identity matrix. In addition to the free evolution, we assume that individual spins can be selectively excited using radio-frequency (rf) pulses, which is the case if the Larmor frequencies of the spins are well separated as compared to the coupling strengths $J_{\ell,\ell+1}$. Thus controls on individual spins can be applied on a much faster time scale as compared to the free evolution with respect to the drift Hamiltonian.

We derive explicit controls for the amplitude and phase of the external rf fields by implementing a unitary evolution

which transforms an initial polarization I_{1x} on the first spin to a multiple-spin state $2^{n-1}(\prod_{\ell=1}^{n-1} I_{\ell y})I_{nz}$ while minimizing the pulse duration t_p. In the following, we often compare control pulses with the *conventional strategy*, which consists of $n-1$ steps of free evolution ($1 \leqslant m \leqslant n-1$)

$$2^{m-1} I_{1y} \cdots I_{(m-1)y} I_{mx} \xrightarrow{H_d} 2^m I_{1y} \cdots I_{my} I_{(m+1)z}$$

where each individual step—besides the final one—is followed by one hard $\frac{\pi}{2}$ pulse on the $(m+1)$th spin along the y direction. As each period of free evolution is of length $1/(2J_{\ell,\ell+1})$ where $J_{\ell,\ell+1}$ is given in hertz, the total evolution time is given by $t_p = \sum_{\ell=1}^{n-1} 1/(2J_{\ell,\ell+1})$.

III. LINEAR THREE-SPIN CHAINS: ANALYTICAL AND NUMERICAL APPROACHES

A. Analytical approach

In this section, we consider the model of Sec. II in the case of linear three-spin chains (see Fig. 1). In the most general case, one could allow independent controls on each of the three spins along both the x and y directions. But in order to simplify the control problem we allow only one control on the second spin along the y direction. This might not lead to time-optimal controls. But even using this restricted model, controls which are shorter as compared to the conventional strategy were obtained in Ref. [12] (see also [11]). In the following, we summarize the analytical approach of Ref. [12].

Starting from an initial state I_{1x} and using only one control on the second spin along the y direction, we can analyze the control problem on the subspace spanned by the operators I_{1x}, $2I_{1y}I_{2z}$, $2I_{1y}I_{2x}$, and $4I_{1y}I_{2y}I_{3z}$ as compared to the full 63-dimensional space of operators. Using the notation $\langle O \rangle := \text{Tr}(O\rho)$ for the expectation value and Tr for the trace, we denote the corresponding expectation values by $x_1 = x_1(t) = \langle I_{1x} \rangle$, $x_2 = x_2(t) = \langle 2I_{1y}I_{2z} \rangle$, $x_3 = x_3(t) = \langle 2I_{1y}I_{2x} \rangle$, and $x_4 = x_4(t) = \langle 4I_{1y}I_{2y}I_{3z} \rangle$. We obtain the differential equation

$$\begin{pmatrix} \dot{x}_1 \\ \dot{x}_2 \\ \dot{x}_3 \\ \dot{x}_4 \end{pmatrix} = \pi \begin{pmatrix} 0 & -1 & 0 & 0 \\ 1 & 0 & -u & 0 \\ 0 & u & 0 & -k \\ 0 & 0 & k & 0 \end{pmatrix} \begin{pmatrix} x_1 \\ x_2 \\ x_3 \\ x_4 \end{pmatrix}, \qquad (3)$$

where $u = u(t)$ denotes the amplitude of the control on the second spin along the y direction and $k = J_{23}/J_{12}$. Using the coordinates $(x_1, x_2, x_3, x_4)^T$ we aim to time-efficiently transfer $(1,0,0,0)^T$ to $(0,0,0,1)^T$.

Now, we change from the coordinates $(x_1, x_2, x_3, x_4)^T$ to the coordinates

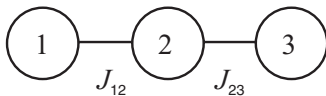$$(r_1, r_2, r_3)^T = \left(x_1, \sqrt{x_2^2 + x_3^2}, x_4 \right)^T$$

FIG. 1. A linear three-spin chain has only direct couplings J_{12} and J_{23} between neighboring spins.
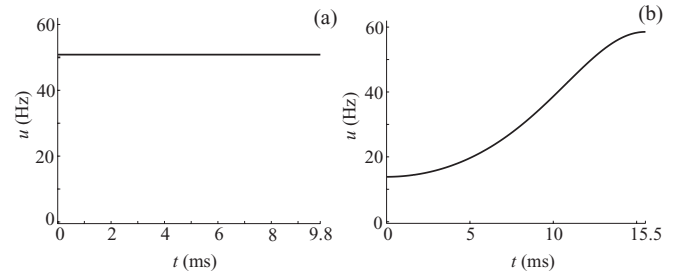

FIG. 2. Analytical pulses for linear three-spin chains in the cases of (a) $k = J_{23}/J_{12} = 88.05/88.05 = 1$ and (b) $k = 1.59 \approx J_{23}/J_{12} = 73.1/46$.

on the sphere where $\theta = \theta(t)$ is given by $\tan\theta = x_3/x_2$. This transforms Eq. (3) to

$$\begin{pmatrix} \dot{r}_1 \\ \dot{r}_2 \\ \dot{r}_3 \end{pmatrix} = \pi \begin{pmatrix} 0 & -\cos\theta & 0 \\ \cos\theta & 0 & -k\sin\theta \\ 0 & k\sin\theta & 0 \end{pmatrix} \begin{pmatrix} r_1 \\ r_2 \\ r_3 \end{pmatrix}.$$

In the new coordinates, we want to time-efficiently transfer $(1,0,0)^T$ to $(0,0,1)^T$.

In order to find the time-optimal controls, Euler-Lagrange equations were set up and solved in Ref. [12], leading to the differential equation

$$\ddot{\theta} = \frac{k^2 - 1}{2} \sin 2\theta \qquad (4)$$

for the variable θ. The differential equation (4) can be numerically integrated if the initial values $\theta(0)$ and $\dot{\theta}(0)$ are known. Using the results of Ref. [12] one can determine conditions on the initial values: In the case of $(r_1(0), r_2(0), r_3(0))^T = (1,0,0)^T$ one can deduce that $\theta(0) = 0$, but $\dot{\theta}(0)$ is undetermined. In Ref. [12] combinations of one-dimensional searches were used to determine the optimal $\theta_{\text{opt}}(t)$ and the time-optimized control as $u_{\text{opt}}(t) = J_{12}\dot{\theta}_{\text{opt}}(t)$. Examples for the corresponding (semi)analytic pulses are shown in Fig. 2. The values are motivated by the experimental systems given in Fig. 3.
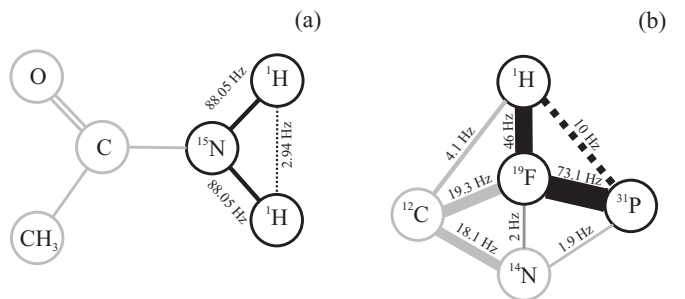

FIG. 3. The schematic coupling topologies of (a) ethanamide and (b) diethyl-(dimethylcarbonyl)fluoromethylphosphonate (see [67,68]) result in experimental three-spin systems with coupling ratios (a) $k = 1 = 88.05/88.05$ and (b) $k = 1.59 \approx 73.1/46$. Larger couplings are shown as solid black lines, and smaller couplings are shown as dashed black lines. Decoupled spins are given in gray color.

B. Numerical approach

We numerically optimize pulse shapes by employing the GRAPE algorithm [48] which was developed by applying principles of optimal control theory. Using a gradient-based optimization, we obtain rf controls which steer an initial state (or unitary transformation) to a final state (or unitary transformation) while minimizing (e.g.) the duration of the pulse. Both the amplitude and the phase of the resulting pulse can have a smooth or noisy shape depending on (e.g.) the initial pulse or bounds on the control strength (see, e.g., [63]).

We treat three different levels of rf controls: First, we use only one rf control operating on the second spin along the y direction. Second, we use two different rf controls operating on the second spin along both the x and y directions. Third, we use a total of six rf controls operating on each of the three spins along both the x and y directions. We remark that employing rf controls on one spin along both the x and y directions gives complete (local) control on that spin. Let k denote the ratio between the couplings J_{23} and J_{12}. We determine the numerically optimized pulses and plot the logarithmic fidelity F vs the duration t_p of differently shaped pulses for the coupling ratios $k = 1$ and $k = 1.59$ which are motivated by the experimental scenarios of Fig. 3. The numerical results are given in Table I:

TABLE I. We compare the duration t_p, the logarithmic fidelity $\log(1 - F) := \log_{10}(1 - F)$, and the shape of numerically optimized pulses for a linear three-spin chain with coupling ratios (a) $k = 1$ and (b) $k = 1.59$. The number of controls is given in the first column. In the third column we present the corresponding logarithmic TOP curves. The second column shows an example of a shaped pulse which corresponds to the the shortest pulse with fidelity $F \geqslant 0.9999$ (unless otherwise stated) and whose position is denoted with an x in the logarithmic TOP curve. The rf control on the middle spin along the y axis is plotted using a solid black line. Other rf controls are plotted using dashed or solid gray lines. All logarithms are to base 10.
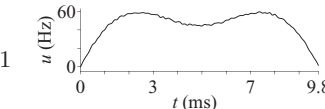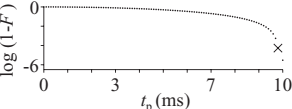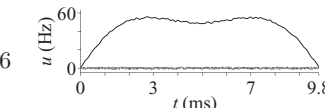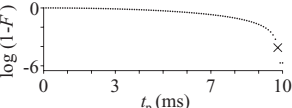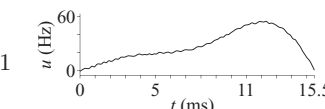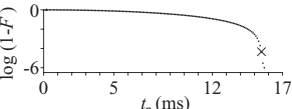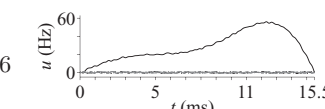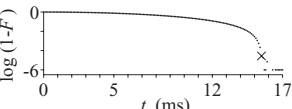
No. of controls	Pulse shape	Logarithmic TOP curve

TABLE II. For coherence transfers in linear three-spin chains ($k = 1$ and 1.59), we give the numerically optimized times t_p and the fidelities F in the cases of one, two, and six rf controls (see text). The duration t_p is independent of the number of controls, which suggests that only one rf control on the middle spin is sufficient for the time-optimal coherence transfer.

k	No. of controls	t_p (ms)	F
1	1	9.8	0.999 95
1	2	9.8	0.999 92
1	6	9.8	0.999 92
1.59	1	15.5	0.999 95
1.59	2	15.5	0.999 96
1.59	6	15.5	0.999 97

We show examples of shaped pulses of duration t_p which correspond to the the shortest pulse with fidelity $F \geqslant 0.9999$ (unless otherwise stated). In addition, we present logarithmic time-optimal curves where we plot the logarithmic transfer efficiency [i.e., $\log(1 - F) := \log_{10}(1 - F)$ where F is the fidelity; all logarithms are to base 10] versus the optimal transfer time. Comparison of the different cases suggests that only one rf control on the second spin is sufficient for a time-optimal pulse. For high fidelities ($F \geqslant 0.9999$), the durations of the analytical and numerically optimized pulses are identical (to the given accuracy) while the pulse forms differ. In Table II, we compare the durations of pulses on linear three-spin systems for different values of k.

Conjecture 1. Consider a linear three-spin chain with local controls on each spin. One can time-optimally transfer coherence from I_{1x} to $4I_{1y}I_{2y}I_{3z}$ using only one control on the second spin along the y direction. In addition, the analytical pulses of Refs. [11,12] are time optimal in the case of linear three-spin chains even if one allows arbitrary local controls.

IV. LINEAR FOUR-SPIN CHAINS: ANALYTICAL AND NUMERICAL APPROACHES

A. Analytical approach

In this section, we consider linear spin chains with four spins. We follow Sec. IV of Ref. [12] (see also [11]) and split the control problem for four spins into two subproblems for three spins (see Fig. 4): The first subproblem is given on the first three spins by the time-optimal transfer from $(1,0,0)^T$ to $(0, \cos \gamma, \sin \gamma)^T$, where we are again using the coordinates $(r_1, r_2, r_3)^T$ of Sec. III A. Then, we apply certain (arbitrarily fast) hard pulses which can be easily determined by numerical methods. The second subproblem is given on the last three
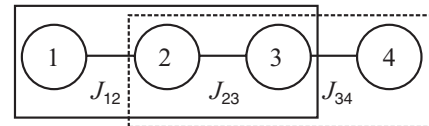

FIG. 4. A linear four-spin chain has only direct couplings J_{12}, J_{23}, and J_{34} between neighboring spins. We split the corresponding four-spin chain control problem into two subproblems for three-spin chains.
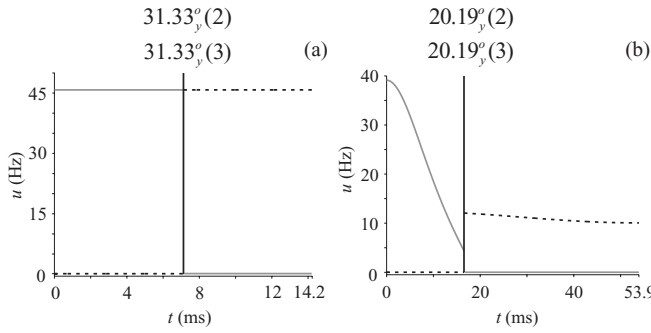
FIG. 5. Analytical pulses for linear four-spin chains are given in the cases of (a) $k_1 = k_2 = 1$ as well as (b) $k_1 = 2.38$ and $k_2 = 0.94$. The pulses on the second and third spins along the y direction are given, respectively, as solid and dashed lines. The corresponding two hard pulses on the second and third spins are depicted by a vertical line with the flip angles given above. The hard pulses in the left figure can be implemented by applying a pulse of 5000 Hz for 17.40 ms. The hard pulses in the right figure can be implemented by applying a pulse of 5000 Hz for 11.21 ms.

spins by the time-optimal transfer from $(\cos\gamma, \sin\gamma, 0)^T$ to $(0,0,1)^T$. In addition, we have to simultaneously search for the value of γ which minimizes the pulse duration. This approach might not lead to time-optimal controls but simplifies the control problem significantly.

The optimization of the considered subproblems can be reduced to time-optimal transfers from $(\cos\alpha, \sin\alpha, 0)^T$ to $(0, \cos\beta, \sin\beta)^T$ for $\alpha, \beta \in [0, \pi/2]$, generalizing the transfer of Sec. III A from $(1,0,0)^T$ to $(0,0,1)^T$. Using methods of Ref. [12] we can find the optimal controls for the transfers using combined one-dimensional searches for the optimal initial values $\theta(0)$ and $\dot\theta(0)$ of Eq. (4). Both $\theta(0)$ and $\dot\theta(0)$ are undetermined but related by $\dot\theta(0) = \sin[\theta(0)] \cot\alpha$ for the case of $(r_1(0), r_2(0), r_3(0))^T = (\cos\alpha, \sin\alpha, 0)^T$. The corresponding (semi)analytic pulses are shown in Fig. 5. The values are motivated by the experimental system given in Fig. 6.

B. Numerical approach

Motivated by the analytical approach, we numerically treat the control problem on four spins with two cases of coupling ratios (a) $k_1 = 1$ and $k_2 = 1$ ($J_{12} = J_{23} = J_{34} = 88.05$ Hz), and (b) $k_1 = 2.38 \approx J_{12}/J_{23}$ and $k_2 = 0.94 \approx J_{34}/J_{23}$ (refer
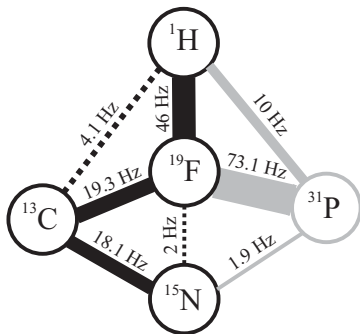

FIG. 6. The topology of the molecule ^{13}C^O-^{15}N-diethyl-(dimethylcarbonyl)fluoromethylphosphonate (see [67,68]) results in coupling ratios $k_1 = 2.38$ and $k_2 = 0.94$. Compare to Fig. 3.

TABLE III. For linear four-spin chains with coupling ratios (a) $k_1 = 1$ and $k_2 = 1$ as well as (b) $k_1 = 2.38$ and $k_2 = 0.94$, the rf controls on the second and third spins along the y axis are plotted using solid black and solid gray lines, respectively. Other rf controls are plotted using a dashed black line or in shades of gray. Compare to Table I.

No. of controls	Pulse shape	Logarithmic TOP curve

to Fig. 6 for the coupling values). The coherence transfer is numerically optimized considering the following three levels of rf controls: First, we use only two different rf controls (one on each spin) operating on the second and third spins along the y direction. Second, we use a total of four different rf controls (two on each spin) operating on the second and third spins along both the x and y directions. Third, we use a total of eight different rf controls (two on each spin) operating on each of the four spins along both the x and y directions. The pulse shapes and the logarithmic TOP curves corresponding to two and eight rf controls (see Table III) indicate that we do not gain a higher fidelity or a shorter duration by using more than the two controls (Table IV). This is consistent with the analytical results, but the numerically optimized pulses appear to be a little shorter than the analytical ones (cf. Fig. 5).

Conjecture 2. Consider a linear four-spin chain with local controls on each spin. One can time-optimally transfer coherence from I_{1x} to $8I_{1y}I_{2y}I_{3y}I_{4z}$ using only two controls along the y direction, which operate on the second and third spins, respectively.

We will now discuss the qualitative form of the logarithmic TOP curves as in Table III. It is apparent that some of the (numerically obtained) logarithmic TOP curves are no longer *smooth* after a certain time t_p. First, we want to emphasize that the *logarithmic* TOP curve is plotted using a *logarithmic* scale, giving a better picture of the numerical convergence properties as compared to a normal TOP curve where the nonsmoothness would not even be visible. Second, we usually made no attempt to reoptimize points where the algorithm has (apparently) not fully converged to the global optimum. This allowed us

TABLE IV. For coherence transfers in linear four-spin chains ($k_1 = k_2 = 1$ as well as $k_1 = 2.38$ and $k_2 = 0.94$), we give the numerically optimized times t_p and the fidelities F in the cases of two, four, and eight rf controls. The duration t_p is independent of the number of controls, which suggests that only two rf controls on the second and third spins along the y axis are sufficient for the time-optimal coherence transfer.

k_1	k_2	No. of controls	t_p (ms)	F
1	1	2	13.8	0.999 92
1	1	4	13.8	0.999 93
1	1	8	13.8	0.999 89[a]
2.38	0.94	2	53.2	0.999 90
2.38	0.94	4	53.2	0.999 90
2.38	0.94	8	53.3	0.999 92

[a]Although this fidelity is not larger than 0.9999 (before rounding), one can take the corresponding pulse with two controls, which would achieve $F \geqslant 0.9999$.

to identify the limits of the numerical optimization with the beginning of the nonsmoothness. Third, we are satisfied with a pulse sequence if its fidelity F is larger than or equal to 0.9999 (cf. caption of Table I) and no other, more sophisticated criteria were used (after the numerical optimization). Fourth, we recorded the fidelity using only six decimal digits after the decimal point and we did not analyze effects resulting from this choice. All these decisions were motivated by the fact that we only seek strong numerical evidence for Conjectures 1 and 2 as even the most advanced numerical optimization method could not provide a *proof*.

We show in Fig. 7 different pulse shapes corresponding to the case of eight controls in Table III(b) (see also Table IV). One can see that the pulse shapes usually do not vary much around the fidelity $F = 0.9999$, but pulse shapes as in Fig. 7(c) may appear. We remark that the very strong modulations in Fig. 7(c) are essentially redundant as they correspond approximately to a 2π pulse on spin 3. Note also the pulse shape in Fig. 7(a) which is similar to a reflected version of Fig. 7(e).

V. MORE GENERALLY COUPLED SPIN SYSTEMS OF THREE AND FOUR SPINS

In more generally coupled spin systems, indirect couplings can strongly impede or enhance the coherence transfer. In this section we present detailed numerical optimizations and compare them to the case of linear spin chains.

A. Three-spin system

Along the lines of Sec. III B, we numerically optimize pulses for more generally coupled three-spin systems keeping $J_{12} = J_{23} = 88.05$ Hz constant while varying the additional coupling strength J_{13}. By comparing the TOP curves for different values of J_{13}, we conclude that for a larger coupling strength J_{13} the fidelity of the coherence transfer is smaller in the cases of one [Fig. 8(a)] and two (results are not shown) rf controls on the second spin. (As in Sec. III B, we obtain shorter pulse sequences as compared to the conventional pulse sequence for $J_{13} = 0$.) However, using the rf controls on each of the three spins allows for a coherence transfer with higher
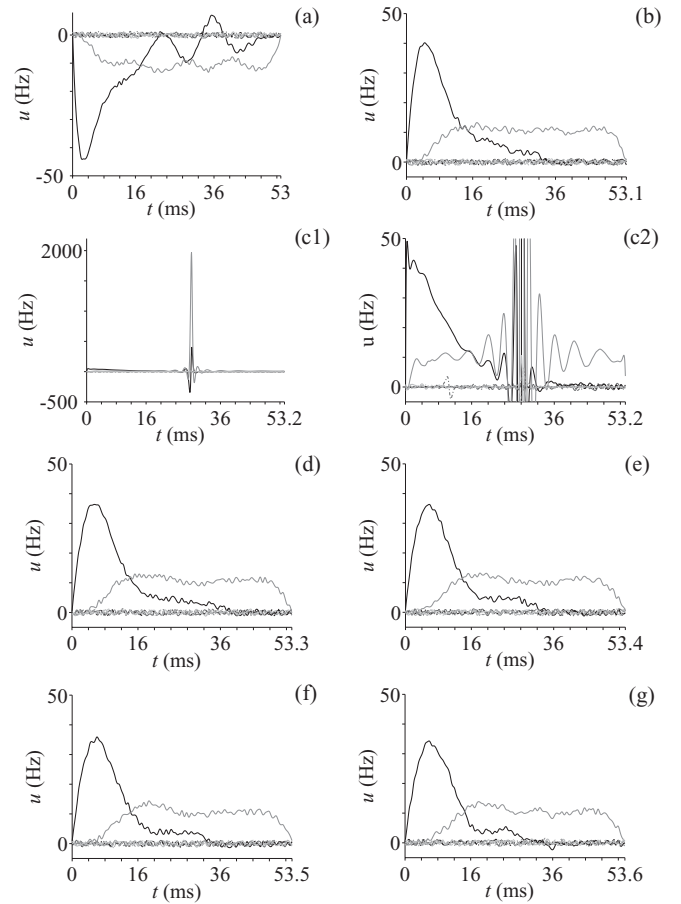

FIG. 7. Different pulse shapes corresponding to the case of eight controls in Table III(b). The pulse shapes (c1) and (c2) are identical but they have been plotted with different scalings to allow for a better comparison. The fidelities for the cases (a)–(g) are (respectively) 0.999 73, 0.999 82, 0.999 15, 0.999 92, 0.999 96, 0.999 98, and 1.000 00 (which are rounded to five decimal digits after the decimal point).

fidelity while keeping the pulses short [Fig. 8(b)]. Table V shows examples of shaped pulses and the corresponding logarithmic TOP curves for the coupling ratios $k = 1$ and 1.59. The coupling strengths are taken from the spin systems shown in Fig. 3. Detailed values are given in Table VII.

B. Four-spin system

Following Sec. IV B, we numerically optimize the shaped pulses for more generally coupled four-spin systems. Analyzing the numerical results (see Table VI), we can say that this system needs all eight rf controls on each spin along both the x and y directions in order to achieve the coherence transfer with minimum duration and maximal fidelity. Table VII summarizes and compares the duration t_p and fidelity F of shaped pulses for more generally coupled spin systems.

VI. EXPERIMENTAL RESULTS

Analytical and numerically optimized pulses are usually optimized for on-resonance cases. We follow the DANTE approach [65,66,69] in order to obtain pulses which are
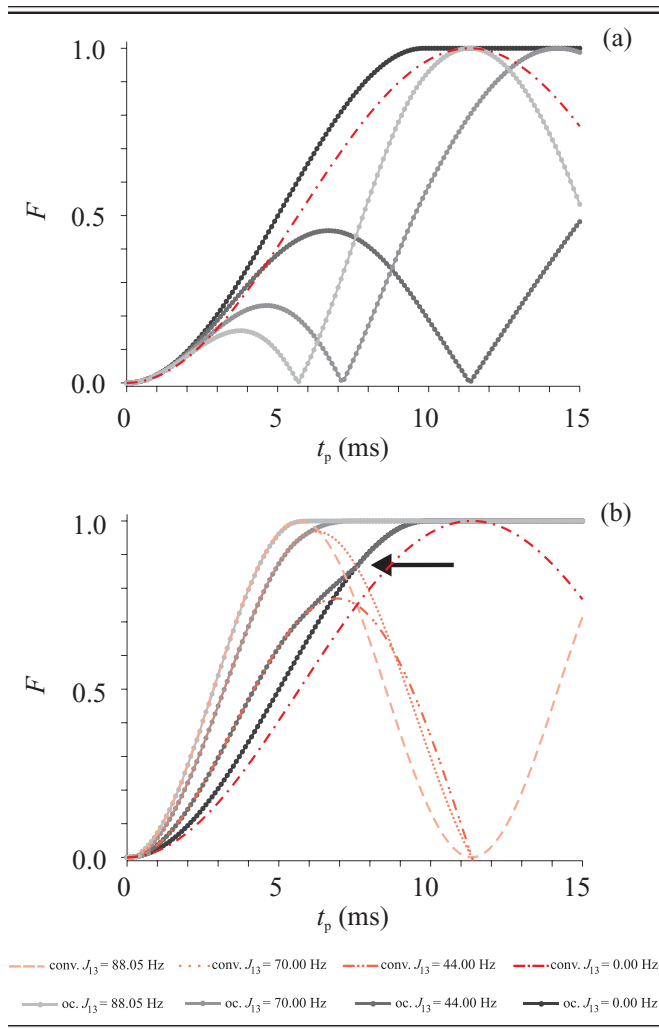
FIG. 8. (Color online) We compare numerically optimized TOP curves (in shades of gray and denoted by oc. in the legend) for three-spin systems with one (a) and six (b) rf controls keeping $J_{12} = J_{23} = 88.05$ Hz constant while varying J_{13}. At the same time we compare their performance with conventional pulse sequences (in shades of red and denoted by conv. in the legend) where both of the couplings J_{12} and J_{13} evolve simultaneously. The limiting case of $J_{13} = 0$ corresponds to the conventional pulse sequence of Sec. II. Using all six rf controls (b), we can see higher fidelities F for smaller times and larger J_{13} compared to the case of only one rf control (a). A black arrow denotes where the numerically optimized TOP curves for $J_{13} = 44$ Hz and $J_{13} = 0$ Hz merge.

broadband, i.e., invariant with respect to the change of the chemical shift in a given offset range (Fig. 9). First, a shaped pulse is converted into a sequence of short hard pulses and delays. We used hard pulses with constant flip angles (see below), and the delays between the hard pulses correspond to the time required by the shaped pulse to accumulate this flip angle [65,66,69]. Then, a refocusing element (i.e., π pulse) [34,66] is inserted between two hard pulses. The offset bandwidth covered by a refocused DANTE sequence is directly proportional to the rf amplitude of the applied hard and π pulses.

TABLE V. Numerical results for more generally coupled three-spin systems with (a) coupling ratio $k = 1$ (i.e., $J_{12} = J_{23} = 88.05$ Hz) and additional coupling $J_{13} = 2.94$ Hz as well as (b) coupling ratio $k = 1.59$ (i.e., $J_{12} = 73.1$ Hz and $J_{23} = 46$ Hz) and additional coupling $J_{13} = 10.0$ Hz. The values of the fidelities can be found in Table VII. Compare to Table I.
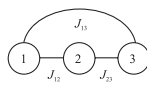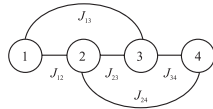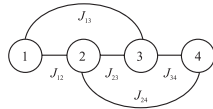

All the experiments are implemented on a Bruker AVANCE III 600 MHz spectrometer at 298 K: We use a triple-resonance TXI probe head with Z gradient in the case of the three-spin system with $k = 1$. For the three-spin system with $k = 1.59$ and the four-spin system with $k_1 = 2.38$ and $k_2 = 0.94$, we use a custom-made six-channel probe head with Z gradient addressing all nuclei ^{19}F, ^{1}H, ^{31}P, ^{12}C (or ^{13}C), and ^{14}N (or ^{15}N) (see [67,68]). In the experiments for three spins we use the molecules shown in Fig. 3. The experiment for the

TABLE VI. Numerical results for more generally coupled four-spin systems with coupling ratios $k_1 = 2.38 \approx J_{12}/J_{23}$ and $k_2 = 0.94 \approx J_{34}/J_{23}$ (i.e., $J_{12} = 46$ Hz, $J_{23} = 19.3$ Hz, and $J_{34} = 18.1$ Hz) as well as additional couplings $J_{13} = 4.1$ Hz and $J_{24} = 2$ Hz. The values of the fidelities can be found in Table VII. In this case, many additional numerical optimizations were done as many of the optimizations have a fidelity close to $F \geqslant 0.9999$. Compare to Table III.

TABLE VII. We compare the duration t_p and fidelity F of numerically optimized shaped pulses in the cases of three- and four-spin systems allowing a varying number of rf controls u. Using only one or two rf controls, we show the effect of indirect couplings—which are usually present in experiments—on the fidelity of optimized pulses with the same pulse duration. Hence more (i.e., six or eight) rf controls are necessary for higher fidelities. The J values are taken from the actual spin systems shown in Figs. 3 and 6.

Graph	J_{13} (Hz)	J_{24} (Hz)	No. of controls	t_p (ms)	F
			$k = 1$		
	0.0	–	1	9.8	0.99995
	2.9	–	1	9.8	0.99596
	2.9	–	6	10.1	0.99990
			$k = 1.59$		
	0.0	–	1	15.5	0.99995
	10.0	–	1	14.7	0.88905
	10.0	–	1	15.5	0.88372
	10.0	–	6	15.8	0.99995
			$k_1 = 2.38$ and $k_2 = 0.94$		
	0.0	0.0	2	53.2	0.99990
	4.1	2.0	2	53.2	0.98593
	4.1	2.0	2	57.8	0.99981
	4.1	2.0	2	66.0	0.99993
	4.1	2.0	8	53.2	0.99884
	4.1	2.0	8	54.0	0.99975
	4.1	2.0	8	63.0	0.99991

coupling ratio $k = 1$ uses the first molecule [see Fig. 3(a)] which is dissolved in deuterated water D_2O. For $k = 1.59$ we use the second molecule [see Fig. 3(b)] dissolved in deuterated methanol CD_3OD. The simulated and experimental offset profiles are shown in Figs. 10 and 11. We emphasize that the duration of the broadband versions of the analytical or the numerically optimized pulses is shorter than for the conventional pulse sequence while keeping its robustness.
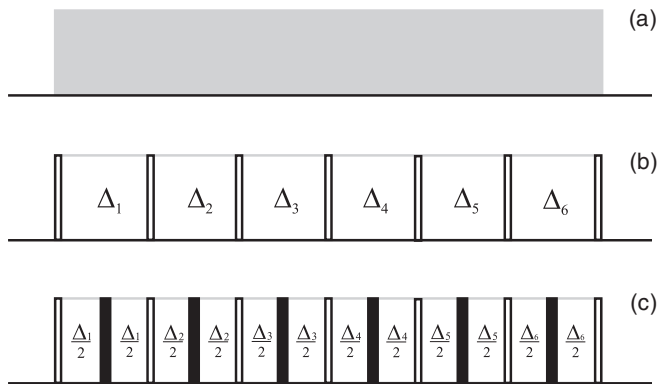

FIG. 9. In the DANTE approach an on-resonance shaped pulse [see (a)] is converted to a series of short hard pulses and delays Δ_i [see (b)]. Then the pulse can be converted to a broadband pulse by inserting a refocusing element (i.e., π pulse) represented by solid bars between two hard pulses [see (c)].
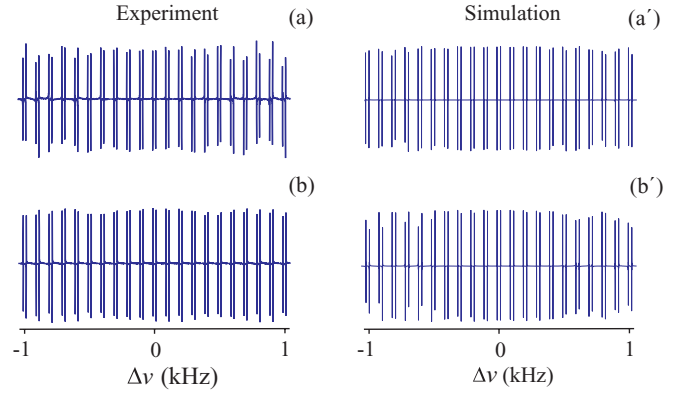

FIG. 10. (Color online) We compare for a three-spin system the offset ($\Delta\nu$) profile for ± 1 kHz of the antiphase signal (see text) resulting from a conventional pulse sequence ($t_p = 11.4$ ms) in the case of experiment [see (a)] and simulation [see (a′)] with broadband versions of the analytical pulses [$t_p = 9.8$ ms; see (b) and (b′)] for the case of coupling ratio $k = 1$ of three spins.

We first discuss the two three-spin systems: In the case of $k = 1$, we start from the initial polarization I_{1z} of ^{1}H (which models the first spin) and apply a $\frac{\pi}{2}$ pulse along the $+y$ direction in order to obtain the coherence I_{1x}. By applying a broadband version of our shaped pulse to the spin of ^{15}N (which models the second spin) we get the three-spin coherence $4I_{1y}I_{2y}I_{3z}$. The broadband version of this shaped pulse is divided into four hard pulses with an amplitude of 4145.936 Hz, a flip angle of 45.00°, and zero phase; it also contains refocusing π pulses where the phases are chosen according to the MLEV-4 cycle [70]. Next, we apply a $\frac{\pi}{2}$ pulse on ^{15}N along the x direction and we obtain the coherence $4I_{1y}I_{2z}I_{3z}$. In the end, we can detect an antiphase signal of ^{1}H (first spin) with respect to the spins of ^{15}N and ^{1}H (which models the third spin). Similarly, in the case of $k = 1.59$, we start from the initial coherence I_{1z} on the spin of ^{1}H (which models the first spin) and apply a $\frac{\pi}{2}$ pulse along the $+y$ direction in order to obtain the coherence I_{1x}. Then, we apply the broadband version of our shaped pulse on the spin of ^{19}F (second spin) in order to produce the three-spin coherence $4I_{1y}I_{2y}I_{3z}$. The broadband version of this shaped pulse is divided into four hard pulses with an amplitude of 10 000 Hz, a flip angle of 45.03°, and zero phase; it also contains refocusing
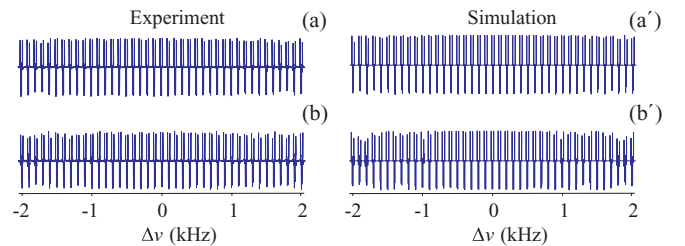

FIG. 11. (Color online) We compare for a three-spin system the offset ($\Delta\nu$) profile for ± 2 kHz of the antiphase signal (see text) resulting from a conventional pulse sequence ($t_p = 17.7$ ms) in the case of experiment [see (a)] and simulation [see (a′)] with broadband versions of the analytic pulses [$t_p = 15.5$ ms; see (b) and (b′)] for the case of coupling ratio $k = 1.59$.
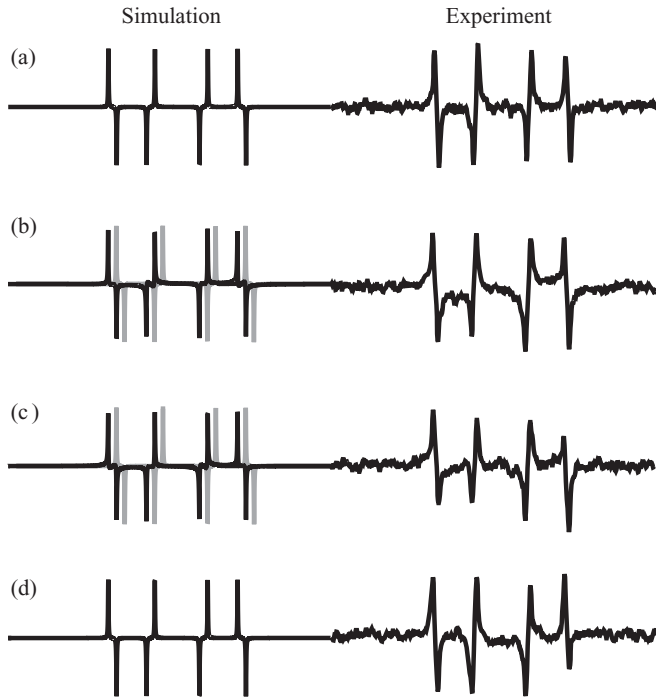
FIG. 12. We show the antiphase signal of the spin of ^{19}F with respect to the spins of ^{1}H, ^{13}C, and ^{15}N of a four-spin system corresponding to the simulation (left) and experiment (right). We use the conventional pulse sequence (a) ($t_p = 64.4$ ms), an analytical pulse sequence (b) ($t_p = 53.9$ ms), a pulse which was numerically optimized for the abstract linear spin chain with rf controls on the second and third spins (c) ($t_p = 53.2$ ms), and a pulse which was numerically optimized for the more generally coupled spin system with rf controls on all spins (d) ($t_p = 54.0$ ms). The simulation for the abstract linear spin chain is given in gray color. All the other plots for the more realistic case of a more generally coupled spin system are given in black color. The plots are scaled vertically by a factor of 2.

π pulses where the phases are chosen according the MLEV-4 cycle [70]. In the next step, we apply a $\frac{\pi}{2}$ pulse on the spin of ^{1}H and we end up with the coherence $4I_{1z}I_{2y}I_{3z}$. Finally, we detect an antiphase signal on the spin of ^{19}F with respect to the spins of ^{1}H and ^{31}P (which models the third spin).

TABLE VIII. We compare the minimum time t_p required for a coherence transfer by numerically optimized (oc) and conventional (conv) pulse sequences for different numbers n of spins and coupling ratios k.

| | $t_p(s)$ | | | | | |
| | $k = 1$ | | | $k \neq 1$[a] | | |
n	oc[b]	conv	oc/conv	oc[b]	conv	oc/conv
3	0.0098	0.0114	0.8596	0.0155	0.0177	0.8757
4	0.0138	0.0170	0.8118	0.0532	0.0644	0.8261
5	0.0177	0.0227	0.7797			
6	0.0216	0.0284	0.7605			

[a]For $n = 3$ we have $k = 1.59$. And for $n = 4$ we have $k_1 = 2.38$ and $k_2 = 0.94$.
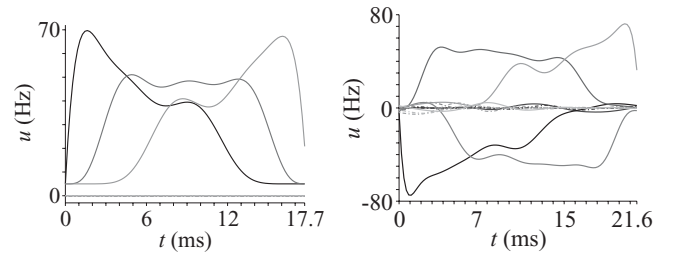[b]The fidelities of the numerically optimized sequences are given as $F \geqslant 0.9999$.

FIG. 13. Using all ten (or twelve) rf controls we determined numerically optimized pulse shapes for linear spin chains of length 5 (or 6) in the case of $k = 1$. We remark that most control strengths are very small.

In the four-spin system, we show on-resonance simulations and experiments for numerically optimized shaped pulses, comparing the conventional approach with analytical and numerically optimized pulses (see Fig. 12). The corresponding experiments are implemented on the molecule of Fig. 6, which is dissolved in deuterated acetonitrile. Figures 12(b) and 12(c) show a reduction in signal intensity for the simulation if we compare the effect of the pulse on the abstract linear spin chain (shown in gray) with the effect on the more realistic and more generally coupled spin system (shown in black) as the corresponding pulses were only optimized for the abstract linear spin chain. We remark that the pulse of Fig. 12(d) is optimized for a more generally coupled spin system while using rf controls on all spins. Thus, we conclude—using also the data of Table VII—that the pulse of Fig. 12(d) shows a higher fidelity when compared to the pulses of Figs. 12(b) and 12(c). Furthermore, the pulse corresponding to Fig. 12(d) is shorter (by 14%) than the conventional pulse sequence corresponding to Fig. 12(a) while maintaining its robustness to additional couplings (see also Table VIII).

VII. LINEAR SPIN CHAINS WITH MORE THAN FOUR SPINS

In this section, we generalize the numerical optimization of shaped pulses to linear spin chains of five and more spins. Figure 13 shows two examples of the optimized pulse shapes with coupling ratios $k_\ell = 1$ and coupling strengths $J_{\ell,\ell+1} = 88.05$ Hz. These examples suggest that time-optimal controls can be obtained on multiple spins even while irradiating only on the spins 2 to $\ell - 1$ along the y direction (cf. Sec. IV of Ref. [12]). We obtain shorter pulses for the numerically optimized pulses compared to the conventional pulse sequences, as summarized in Table VIII.

VIII. CONCLUSION

In the case of linear three-spin chains we reproduced numerically the previous analytical results [11,12], obtaining the same family of restricted controls by applying pulses only on the second spin along the y axis. The same holds for linear four-spin chains where we also obtain the analytical family of restricted controls by applying pulses only on the second and third spins along the y axis; but the numerically optimized pulses appear to be a little shorter than the analytical ones. For both three and four spins no gain in pulse duration is found

if arbitrary pulse structures are allowed. These observations are summarized in Conjectures 1 and 2. Even for longer spin chains (of up to six coupled spins 1/2) there is some numerical evidence suggesting that the same restricted controls motivated by Refs. [11,12] lead to time-optimal pulses (under unrestricted controls) for linear spin chains of arbitrary length.

Further numerical results are presented for more general and more realistic coupling topologies, for which so far no analytical results are known; but see recent work in Ref. [71]. Compared to linear spin chains, we obtain different pulse structures depending on the number of available controls. We hope that the presented results and conjectures will motivate further analytical work in order to develop a better understanding of time-optimal control sequences for the generation of multispin coherence.

Note that the minimum times for the transfers $I_{1\delta} \rightarrow 2^{n-1} I_{1\epsilon_1} \cdots I_{n\epsilon_n}$ and $2^{n-1} I_{1\epsilon_1} \cdots I_{n\epsilon_n} \rightarrow I_{1\delta}$ are identical ($\delta, \epsilon_k \in \{x,y,z\}$ for $k = 1, \ldots, n$), which is directly relevant for "out and back" experiments and the reconversion of multiple-quantum coherence to detectable single-quantum operators. In the experimental part, we demonstrated that the optimized pulse sequences work in realistic settings under relaxation and experimental imperfections (e.g., inhomogeneity of the control field, miscalibrations, and phase transients). In addition, the pulses can be made broadband using the DANTE approach.

Here we assumed for simplicity that each spin 1/2 can be selectively addressed, which is directly relevant to heteronuclear spin systems but the optimal transfer scheme can also be adapted to homonuclear spin systems. The presented sequences can be directly applied to small molecules and peptides, which is true in particular for the broadband versions. The minimum pulse sequence durations for complete transfer are reduced by up to 24% compared to conventional approaches (see Table VIII). Conversely, for a fixed transfer time significantly improved transfer amplitudes are possible, e.g., for a linear three-spin chain we gain approximately 23% in transfer efficiency when we allow only for half of the transfer time necessary for a complete transfer (cf. Fig. 8). For large proteins, further gains in efficiency are expected if relaxation-optimized pulse sequences can be developed for the specific relaxation superoperator given in the system. Although such sequences are beyond the scope of the present paper, the results on time-optimal sequences presented here provide an important benchmark for relaxation-optimized sequences.

[1] E. Lieb, T. Schultz, and D. Mattis, Ann. Phys. (NY) **16**, 407 (1961).

[2] H. M. Pastawski, G. Usaj, and P. R. Levstein, Chem. Phys. Lett. **261**, 329 (1996).

[3] S. J. Glaser and G. P. Drobny, Chem. Phys. Lett. **181**, 553 (1991).

[4] J. Listerud, S. J. Glaser, and G. P. Drobny, Mol. Phys. **78**, 629 (1993).

[5] S. J. Glaser, J. Magn. Reson., Ser. A **104**, 283 (1993).

[6] S. J. Glaser and J. J. Quant, in *Advances in Magnetic and Optical Resonance*, edited by W. S. Warren, Vol. 19 (Academic Press, San Diego, 1996), pp. 59–252.

[7] R. M. White, *Quantum Theory of Magnetism* (Springer, Berlin, 1983).

[8] D. C. Mattis, *The Theory of Magnetism I, Statistics and Dynamics* (Springer, Berlin, 1988).

[9] Z. L. Mádi, B. Brutscher, T. Schulte-Herbrüggen, R. Brüschweiler, and R. R. Ernst, Chem. Phys. Lett. **268**, 300 (1997).

[10] N. Khaneja and S. J. Glaser, Phys. Rev. A **66**, 060301(R) (2002).

[11] H. Yuan, S. J. Glaser, and N. Khaneja, Phys. Rev. A **76**, 012316 (2007).

[12] H. Yuan, R. Zeier, and N. Khaneja, Phys. Rev. A **77**, 032340 (2008).

[13] F. Yamaguchi and Y. Yamamoto, Appl. Phys. A **68**, 1 (1999).

[14] S. Bose, Phys. Rev. Lett. **91**, 207901 (2003).

[15] S. Bose, Contemp. Phys. **48**, 13 (2007).

[16] S. G. Schirmer and P. J. Pemberton-Ross, Phys. Rev. A **80**, 030301(R) (2009).

[17] A. Kay and P. J. Pemberton-Ross, Phys. Rev. A **81**, 010301(R) (2010).

[18] A. Kay, Int. J. Quantum Inf. **8**, 641 (2010).

[19] D. Burgarth, K. Maruyama, M. Murphy, S. Montangero, T. Calarco, F. Nori, and M. B. Plenio, Phys. Rev. A **81**, 040303 (2010).

[20] M. L. Remerowski, S. J. Glaser, and G. P. Drobny, Mol. Phys. **68**, 1191 (1989).

[21] H. L. Eaton, S. W. Fesik, S. J. Glaser, and G. P. Drobny, J. Magn. Reson. **90**, 452 (1990).

[22] J. Cavanagh, W. J. Fairbrother, A. G. Palmer, and N. J. Skelton, *Protein NMR Spectroscopy: Principles and Practice* (Academic Press, San Diego, 1996).

[23] R. R. Ernst, G. Bodenhausen, and A. Wokaun, *Principles of Nuclear Magnetic Resonance in One and Two Dimensions*, reprinted with corrections (Clarendon Press, Oxford, 1997).

[24] S. J. Archer, M. Ikura, D. A. Torchia, and A. Bax, J. Magn. Reson. **95**, 636 (1991).

[25] M. Sattler, J. Schleucher, and C. Griesinger, Prog. NMR Spectrosc. **34**, 93 (1999).

[26] M. H. Levitt and R. R. Ernst, J. Chem. Phys. **83**, 3297 (1985).

[27] E. Ising, Z. Phys. **31**, 253 (1925).

[28] W. J. Caspers, *Spin Systems* (World Scientific, Singapore, 1989).

[29] G. A. Morris and R. Freeman, J. Am. Chem. Soc. **101**, 760 (1979).

[30] N. Khaneja, R. Brockett, and S. J. Glaser, Phys. Rev. A **63**, 032308 (2001).

[31] T. O. Reiss, N. Khaneja, and S. J. Glaser, J. Magn. Reson. **154**, 192 (2002).

[32] N. Khaneja, S. J. Glaser, and R. Brockett, Phys. Rev. A **65**, 032301 (2002).

[33] N. Khaneja, F. Kramer, and S. J. Glaser, J. Magn. Reson. **173**, 116 (2005).

[34] N. Khaneja, B. Heitmann, A. Spörl, H. Yuan, T. Schulte-Herbrüggen, and S. J. Glaser, Phys. Rev. A **75**, 012322 (2007).

[35] R. Fisher, H. Yuan, A. Spörl, and S. Glaser, Phys. Rev. A **79**, 042304 (2009).

[36] E. Assémat, M. Lapert, Y. Zhang, M. Braun, S. J. Glaser, and D. Sugny, Phys. Rev. A **82**, 013415 (2010).

[37] N. Khaneja, T. Reiss, B. Luy, and S. J. Glaser, J. Magn. Reson. **162**, 311 (2003).

[38] N. Khaneja, B. Luy, and S. J. Glaser, Proc. Natl. Acad. Sci. USA **100**, 13162 (2003).

[39] D. Stefanatos, N. Khaneja, and S. J. Glaser, Phys. Rev. A **69**, 022319 (2004).

[40] D. P. Früh, T. Ito, J.-S. Li, G. Wagner, S. J. Glaser, and N. Khaneja, J. Biomol. NMR **32**, 23 (2005).

[41] D. Stefanatos, S. J. Glaser, and N. Khaneja, Phys. Rev. A **72**, 062320 (2005).

[42] M. Lapert, Y. Zhang, M. Braun, S. J. Glaser, and D. Sugny, Phys. Rev. Lett. **104**, 083001 (2010).

[43] N. C. Nielsen, C. Kehlet, S. J. Glaser, and N. Khaneja, Encyclopedia of Magnetic Resonance **9**, 100 (2010).

[44] T. E. Skinner, T. O. Reiss, B. Luy, N. Khaneja, and S. J. Glaser, J. Magn. Reson. **163**, 8 (2003).

[45] K. Kobzar, B. Luy, N. Khaneja, and S. J. Glaser, J. Magn. Reson. **173**, 229 (2005).

[46] K. Kobzar, T. E. Skinner, N. Khaneja, S. J. Glaser, and B. Luy, J. Magn. Reson. **194**, 58 (2008).

[47] N. I. Gershenzon, T. E. Skinner, B. Brutscher, N. Khaneja, M. Nimbalkar, B. Luy, and S. J. Glaser, J. Magn. Reson. **192**, 235 (2008).

[48] N. Khaneja, T. Reiss, C. Kehlet, T. Schulte-Herbrüggen, and S. J. Glaser, J. Magn. Reson. **172**, 296 (2005).

[49] Z. Tošner, T. Vosegaard, C. T. Kehlet, N. Khaneja, S. J. Glaser, and N. C. Nielsen, J. Magn. Reson. **197**, 120 (2009).

[50] S. Machnes, U. Sander, S. J. Glaser, P. de Fouquières, A. Gruslys, S. Schirmer, and T. Schulte-Herbrüggen, Phys. Rev. A **84**, 022305 (2011).

[51] P. de Fouquieres, S. G. Schirmer, S. J. Glaser, and I. Kuprov, J. Magn. Reson. **212**, 241 (2011).

[52] A. N. Pechen and D. J. Tannor, Phys. Rev. Lett. **106**, 120402 (2011).

[53] M. Lapert, Y. Zhang, M. Braun, S. J. Glaser, and D. Sugny, Phys. Rev. A **82**, 063418 (2010).

[54] K. Kobzar, T. E. Skinner, N. Khaneja, S. J. Glaser, and B. Luy, J. Magn. Reson. **170**, 236 (2004).

[55] J. L. Neves, B. Heitmann, T. O. Reiss, H. H. R. Schor, N. Khaneja, and S. J. Glaser, J. Magn. Reson. **181**, 126 (2006).

[56] N. Pomplun, B. Heitmann, N. Khaneja, and S. J. Glaser, Appl. Magn. Reson. **34**, 331 (2008).

[57] N. Pomplun and S. J. Glaser, PhysChemChemPhys **12**, 5791 (2010).

[58] M. Braun and S. J. Glaser, J. Magn. Reson. **207**, 114 (2010).

[59] N. I. Gershenzon, K. Kobzar, B. Luy, S. J. Glaser, and T. E. Skinner, J. Magn. Reson. **188**, 330 (2007).

[60] M. Lapert, Y. Zhang, S. J. Glaser, and D. Sugny, J. Phys. B **44**, 154014 (2011).

[61] Y. Zhang, M. Lapert, D. Sugny, M. Braun, and S. J. Glaser, J. Chem. Phys. **134**, 054103 (2011).

[62] T. E. Skinner, T. O. Reiss, B. Luy, N. Khaneja, and S. J. Glaser, J. Magn. Reson. **167**, 68 (2004).

[63] T. E. Skinner, K. Kobzar, B. Luy, R. Bendall, W. Bermel, N. Khaneja, and S. J. Glaser, J. Magn. Reson. **179**, 241 (2006).

[64] T. E. Skinner, M. Braun, K. Woelk, N. I. Gershenzon, and S. J. Glaser, J. Magn. Reson. **209**, 282 (2011).

[65] G. A. Morris and R. Freeman, J. Magn. Reson. **29**, 433 (1978).

[66] N. Khaneja, J.-S. Li, C. Kehlet, B. Luy, and S. J. Glaser, Proc. Natl. Acad. Sci. USA **101**, 14742 (2004).

[67] N. Pomplun, Ph.D. thesis, Technische Universität München, 2010.

[68] R. Marx, N. Pomplun, W. Bermel, H. Zeiger, F. Engelke, A. F. Fahmy, and S. J. Glaser (unpublished).

[69] D. Canet, J. Brondeau, and C. Roumestand, J. Magn. Reson. A **117**, 103 (1995).

[70] M. H. Levitt, R. Freeman, and T. Frenkiel, J. Magn. Reson. **47**, 328 (1982).

[71] H. Yuan and N. Khaneja, Phys. Rev. A **84**, 062301 (2011).